catalysts

MDPI

Article

Magnetic Nanoparticles for Photocatalytic Ozonation of Organic Pollutants

Carla A. Orge *, O. Salomé G. P. Soares, Patrícia S. F. Ramalho, M. Fernando R. Pereira and Joaquim L. Faria

Laboratory of Separation and Reaction Engineering—Laboratory of Catalysis and Materials, (LSRE-LCM), Faculdade de Engenharia da Universidade do Porto, Rua Dr. Roberto Frias, 4200-465 Porto, Portugal

* Correspondence: carlaorge@fe.up.pt

Received: 30 July 2019; Accepted: 19 August 2019; Published: 22 August 2019

Abstract: Magnetic nanoparticles (MNP) composed of iron oxide (or other metal–FeO cores) coated with carbon produced by chemical vapour decomposition (CVD) were used in the photocatalytic ozonation of oxamic acid (OMA) which we selected as a model pollutant. The incorporation of Ag and Cu on FeO enhanced the efficiency of the process. The carbon phase significantly increased the photocatalytic activity towards the conversion of OMA. As for the synthesis process, raising the temperature of CVD improved the performance of the produced photocatalysts. The obtained results suggested that the carbon phase is directly related to high catalytic activity. The most active photocatalyst (C@FeO_CVD850) was used in the removal of other compounds (dyes, industrial pollutants and herbicides) from water and high mineralization levels were attained. This material was also revealed to be stable during reutilisation.

Keywords: magnetic materials; chemical vapour deposition; photocatalytic ozonation; organic pollutants

1. Introduction

Photocatalytic ozonation (PCO) results from the combination of two different techniques, and consequently, the potential of pollutant abatement increases since the generation of hydroxyl radicals is promoted [1]. According to the literature, besides direct ozonation in the presence of suitable catalysts under illumination, O_3 can generate hydroxyl radicals ($HO^{\bullet}$) through the formation of ozonide radical ($O_3^{\bullet-}$) in the adsorption layer of the optical semiconductor (SC) where surface holes ($h^+_{[SC]}$) and electrons ($e^-_{[SC]}$) are generated, as described in Equations (1), (2) and (3). The generated $O_3^{\bullet-}$ species rapidly reacts with H^+ to produce the radical $HO_3^{\bullet}$, which evolves to O_2 and $HO^{\bullet}$. The generated $O_3^{\bullet-}$ species quickly reacts with H^+ in the solution to give the $HO_3^{\bullet}$ radical (Equation (4)), which results in O_2 and $HO^{\bullet}$ (Equation (5)).

$$[SC] + h\nu \rightarrow h^+_{[SC]} + e^-_{[SC]} \quad (1)$$

$$O_3 + e^-_{[SC]} \rightarrow O_3^{\bullet-} \quad (2)$$

$$h^+_{[SC]} + H_2O \rightarrow HO^{\bullet} + H^+ \quad (3)$$

$$O_3^{\bullet-} + H^+ \rightleftarrows HO_3^{\bullet} \quad (4)$$

$$HO_3^{\bullet} \rightarrow HO^{\bullet} + O_2 \quad (5)$$

The reaction between O_3 and electrons on the catalyst surface interferes with the recombination of electrons and positive holes. Consequently, a more significant number of radicals are produced,

thereby accelerating the photocatalytic reaction. Several studies have confirmed the synergistic effects of PCO on the degradation and removal of different substances [1,2].

Examining the papers published in recent years, most of the studies reported the use of AEROXIDE© TiO_2 P25 (Evonik), the "gold standard" in photocatalysis [3], during photocatalytic ozonation. On the other hand, magnetic nanoparticles (MNP) gained increasing importance in different areas such as biomedicine/biotechnology [4–6], catalysis [7–9] and water treatment [10–16]. In spite of being widely used as catalyst supports, carbon materials as a catalyst are attracting a great deal of attention [17]. Coating MNP with a layer of different materials improves their stability and introduces new surface properties and functionalities. The use of MNP coated with carbon will enable catalyst recovery by magnetic separation and also take advantage of the catalytic properties of the carbon materials. Magnetic separation to remove the catalyst from liquid solutions eliminates the necessity of centrifugation, filtration or other impractical techniques for recycling the catalysts, avoiding their agglomeration and consequently increasing their durability [9].

Although the use of MNP has been extensively reported, the development of new catalysts with magnetic properties for application in a wide range of expertise fields is still a challenge. In the case of advanced oxidation processes (AOPs), the use of MNP has also been a subject of intense research, but few works reported the presence of MNP during PCO. Mahmoodi used $CuFe_2O_4$ MNP to study the degradation of a dye in aqueous solution, and his results showed that these nanoparticles are very efficient in the degradation of the selected pollutant [14]. Mahmoodi et al. also investigated PCO for the removal of dyes using nickel–zinc ferrite (NZFMN) nanoparticles and 100% effective removal was verified [15]. Magnetic $ZnFe_2O_4$–C_3N_4 hybrids prepared by a simple reflux treatment were applied in photo-Fenton discolouration of Orange II [18]. Yin et al. [16] used $BiFeO_3$ magnetic nanoparticles as a visible light photocatalyst in the coupling of PCO for the degradation of oxalic acid and norfloxacin. A notable improvement allied to excellent stability during reuse reactions was confirmed. Recently, Hussan et al. [19] verified a high catalytic activity, stability and reuse of $BiFeO_3$ magnetic nanoparticles during aniline degradation. $CoFe_2O_4$ particles with a predominantly mesoporous structure containing a large surface area showed a higher decolourization and mineralization of melanoidin (aminocarbonyl complex polymers containing a dark brown colour present in several distillery wastewaters) during catalytic ozonation [20]. The improvement when compared to O_3 alone was attributed to the generation of $HO^{\bullet}$ radicals in the reaction medium. Magnetic Fe_2O_3 supported on ordered mesopours silica material (SBA-15) was synthesized by a facile impregnation and calcination method and the photocatalytic activities were also evaluated on the degradation of rhodamine B [21]. The structure and amount of catalyst and the concentration of H_2O_2 and the pollutant were the main influencing factors on the degradation of rhodamine B. The prepared magnetic Fe_2O_3/SBA-15 had excellent reusability and stability, showing only a slightly decrease after five consecutive runs. Catalytic ozonation of di-n-butyl phthalate (DBP) was carried out in the presence of Ag-doped $MnFe_2O_4$ catalysts [22]. The Ag-doped $MnFe_2O_4$ enhanced the apparent rate constants compared to O_3 alone and undoped $MnFe_2O_4$ systems, and the catalyst surface hydroxyl groups were identified as a critical factor. The Bi_2WO_6–FeOx photocatalysts presented with stable photocatalytic activity during repetitive norfloxacin degradation experiments [22]. Ortiz-Quiñonez et al. showed that MNP containing Ni prepared by a low-temperature solution combustion method were very active catalysts for the degradation of 4-nitrophenol in aqueous media [23]. Magnetic Fe_3O_4/SnO_2 nanocomposites with different molar ratios were tested in the photodegradation of crystal violet [24]. The photoconductivity studies revealed the ohmic nature of the samples was responsible for the good photocatalytic activity due to the extended photoresponsive range and increase in charge separation rate. A novel rattle-type magnetic Fe_3O_4@Ag@H–BiOCl nanocomposite was successfully prepared by a solvothermal method and evaluated by the photocatalytic degradation of rhodamine B and the antibiotic ciprofloxacin [25]. The characterization results showed that the composites exhibit an obvious cavity that promotes excellent adsorption, showing better performance than pure BiOCl.

The aim of this work is to evaluate the PCO performance of MNP composed of iron oxide and coated with carbon by chemical vapour decomposition (CVD). Oxamic acid (OMA) was selected as a model compound since it is a simple molecule and one of the common final products that result from the degradation of a wide range of pollutants with high refractory character to oxidation [26]. Non-catalytic combined treatment (photo-ozonation), non-catalytic individual processes (single ozonation and photolysis), and the corresponding catalytic individual processes (catalytic ozonation and photocatalysis) were also carried out to understand the reaction mechanisms and evaluate the presence of synergetic effects during OMA removal by PCO. The catalytic activity of the prepared materials was confirmed in the degradation of other pollutants (Colour Index Reactive Blue Dye 5—DYE; aniline—ANL; metolachlor—MTLC) using the most active photocatalysts.

2. Results

2.1. Catalyst Characterisation

Table 1 displays the Brunauer–Emmet–Teller (BET) surface area and the amount of carbon (C) of the prepared samples. The textural characterisation of MNP revealed that the incorporation of Cu or Co in Fe_3O_4 (sample FeO) during the synthesis of these samples increased the BET surface area in contrast with the introduction of Ag that slightly decreased this value. This decrease may rely on the use of the incipient wetness impregnation method to deposit Ag on the FeO surface. In the case of MNP coated with carbon by CVD, we calculated the surface area per gram of carbon previously determined by thermogravimetric (TG) analysis. A drastic decrease to values lower than 10 $m^2\ g^{-1}$ was observed in the surface area of MNP coated by CVD. This decrease is due to the heat treatments used during synthesis, namely the heating up to 400 °C to carry out the reduction of the metal under hydrogen and, after that, a temperature increase up to 750 °C or 850 °C to coat the MNP with carbon [13].

Table 1. Brunauer–Emmet–Teller (BET) surface area (S_{BET}) and amount of carbon. CVD = chemical vapour decomposition.

Sample	S_{BET} ($m^2\ g^{-1}$) (±10 $m^2\ g^{-1}$)	% C †
FeO	154	0
CoFeO	184	0
Cu FeO	235	0
AgFeO	134	0
C@FeO_CVD750	63 *	16
C@FeO_CVD850	29 *	35
C@CoFeO_CVD750	29 *	34
C@CoFeO_CVD850	33 *	43
C@CuFeO_CVD750	27 *	67
C@CuFeO_CVD850	16 *	63
C@TiFeO_met1_CVD850	25 *	20
C@TiFeO_met2_CVD850	26 *	33

* per gram of carbon. † determined by thermogravimetric (TG) analysis.

In general, materials prepared by CVD at 850 °C had a higher amount of carbon than those at 750 °C.

In the transmission electron microscopy (TEM) of selected samples (Figure 1), it is possible to see that MNP are composed of small spheres that are not well defined and have no clear distinction of the different metals, which is indicative of a good dispersion of both metals. TEM images confirm the covering of the MNP with carbon during the CVD process. In the samples C@FeO_CVD750 and C@FeO_CVD850, we can confirm that iron oxide particles are encapsulated (coated with carbon nanotubes and nanofibers). The results suggest that the increase in temperature increased the formation of carbon, as confirmed by the TG analysis. In the case of C@CoFeO_CVD750, MNP are covered by few

carbon layers and also by carbon nanotubes and nanofibers, while C@CoFeO_CVD850 appeared to be encapsulated by carbon nanotubes and nanofibers. Most of the MNP were encapsulated by carbon, but some metal oxide is exposed on the surface.

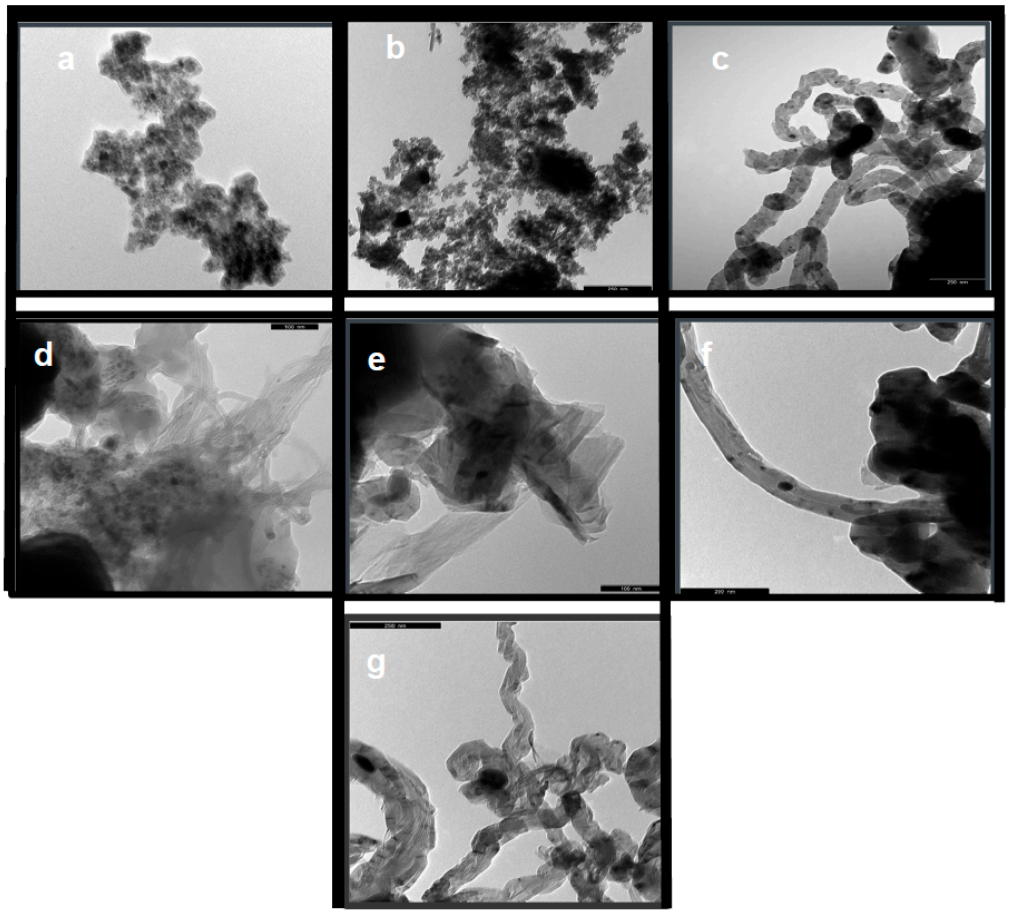

Figure 1. Transmission electron microscopy (TEM) micrographs of selected samples: (**a**) FeO; (**b**) AgFeO; (**c**) C@FeO_CVD750; (**d**) C@FeO_CVD850; (**e**) C@CoFeO_CVD750; (**f**) C@CoFeO_CVD850; (**g**) C@TiFeO_met2_CVD850.

The crystal structure of the prepared MNP was studied by X-ray diffraction (XRD) and the spectra of some of the tested catalysts are depicted in Figure 2. In Table 2, we show the identification of the phases identified in the MNP materials, along with the crystallite sizes. XRD analyses show that the only phase present in the FeO sample is magnetite. The main crystalline phase of AgFeO is also magnetite (92.6%). As expected, the coated MNP have a large amount of carbon in their composition, appearing as graphite with a percentage between 84% and 96%.

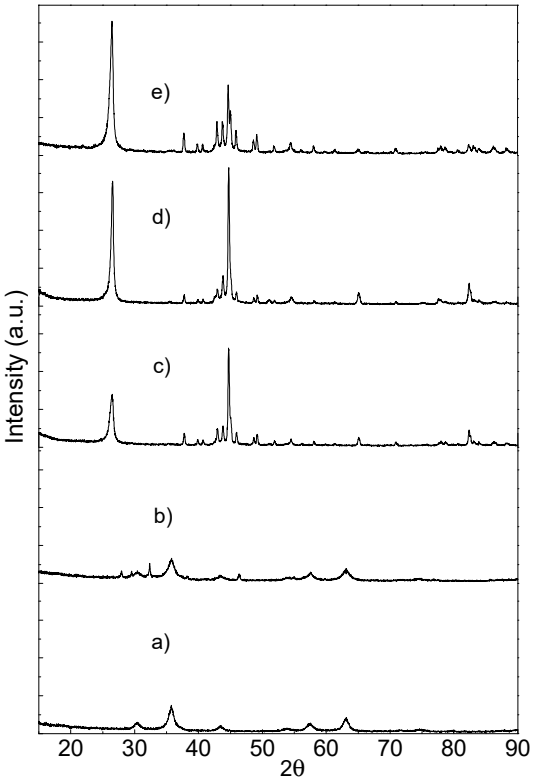

Figure 2. X-ray diffraction (XRD) spectra of selected samples: (**a**) FeO; (**b**) AgFeO; (**c**) C@FeO_CVD750; (**d**) C@CoFeO_CVD850; (**e**) C@TiFeO_met2_CVD850. a.u.: arbitrary units; 2θ: angle between transmitted beam and reflected beam.

Table 2. Properties of selected materials obtained by XRD analysis.

Sample	Phase (%vol/vol)	Crystallite Size (nm) ±6%
FeO	100% magnetite (Fe_3O_4)	20.5
$AgFe_3O_4$	7.3% chlorargyrite (AgCl)	-
	92.6% magnetite (Fe_3O_4)	8.2
C@FeO_CVD750	3% cementite (Fe_3C)	84
	1.6% Fe α	72
	95.4% graphite	16
C@FeO_CVD850	3% cementite (Fe_3C)	52
	1.5% Fe α	73
	95.5% graphite	27
C@TiFeO_met2_CVD850	14.1% cementite (Fe_3C)	72
	2.3% Fe α	10
	83.6% graphite	-

2.2. OMA Removal by MNP

The conversion of OMA by PCO in the presence of different MNP is displayed in Figure 3 (ratio of pollutant concentration/initial pollutant concentration, C/C_0, in function of the time, t). The non-catalytic run was also performed, as well as the individual methods in the absence of catalyst, single ozonation and photolysis as control experiments.

All tested catalysts performed better than the non-catalytic run. The incorporation of Ag and Cu in FeO particles increased the catalytic activity, while the introduction of Co slightly decreased the performance. Although the introduction of Ag in FeO particles reduced the BET surface area,

this sample had the highest OMA removal rate, suggesting that the addition of Ag leads to an increase in activity. Sampaio et al. [27] also observed increased efficiency in phenol degradation in the presence of ZnO loaded with Ag. The authors suggested that there is an optimal amount of Ag to generate an adequate quantity of holes and electrons, and an increase in the Ag load may lead to a surplus charge separation, which is not efficiently contributing to the reaction.

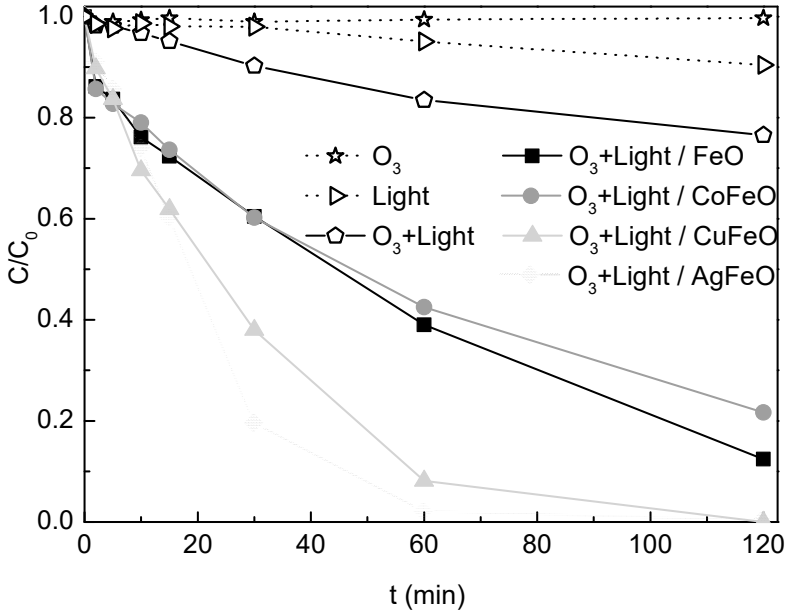

Figure 3. Conversion of oxamic acid (OMA) by photocatalytic ozonation (PCO) in the presence of magnetic nanoparticles (MNP).

2.3. OMA Removal by Carbon Coated MNP by Using 750 °C CVD

FeO, CuFeO and CoFeO particles were coated with carbon by CVD at 750 °C and tested in the removal of OMA by PCO. The conversions of OMA in the presence of several MNP observed up to 120 min of reaction are shown in Figure 4.

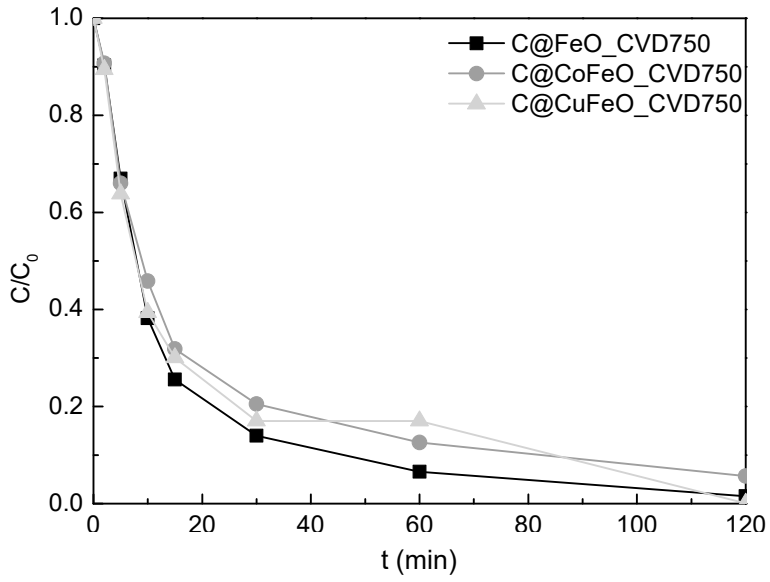

Figure 4. Conversion of OMA by PCO in the presence of MNP coated by CVD at 750 °C.

All MNP coated with carbon by CVD at 750 °C showed better performance than the corresponding uncoated MNP. This result suggests that the carbon phase plays a vital role during PCO, increasing the catalytic activity. However, there are no significant differences among the samples prepared by CVD at 750 °C (Figure 4). The introduction of Co or Cu in FeO particles followed by a CVD treatment at this temperature did not improve the OMA removal rate. The slight increase verified in the C/C_0 value at 60 min during the PCO with C@CuFeO_CVD750 is within the experimental error (<±2%). As observed in the TEM micrographs, MNP were encapsulated by carbon after the CVD treatment, suggesting that the carbon phase is mainly responsible for the improvement in activity. This result is in line with the fact that the presence of the carbon phase reduces the electron/hole recombination due to the formation of solid–solid interfaces that facilitate charge transfer and spatial separation, and improves interfacial defect sites that act as "hot spots" [28]. It is expected that the carbon phase, due to its electric conductivity, acts as photosensitizer to promote electric charge transfer, since it can enhance electron diffusion and reduce electron/hole recombination, and consequently the catalytic activity is improved.

2.4. OMA Removal by Carbon Coated MNP by Using 850 °C CVD

FeO, CoFeO and CuFeO coated with carbon by CVD at a higher temperature, 850 °C, were tested in the same degradation of OMA by PCO (Figure 5a). Because the catalysts are more active, the running time of the experiments was cut down to only 60 min, half of the time of the runs in the presence of the 750 °C CVD coated materials. The increase of the CVD temperature produced a positive effect on the catalytic performance during OMA removal. All MNP coated at 850 °C achieved complete OMA removal after 60 min of reaction. In general terms, the result correlates with the amount of deposited carbon to attain a specific coverage of the MNP. The limit value should lie around the 67% obtained for the Cu modified catalysts. Therefore, besides a thermal effect, the coating requires a certain amount of carbon to become more efficient. Temperatures above 850 °C were outside our experimental range, but there is no significant expected increase in carbon mass production above these temperatures, judging from experience in growing carbon nanotubes by CVD [29].

Taking advantage of the pronounced photoactivity of the Ti-modified materials, we used the TiFeO particles coated with carbon by CVD at 850 °C to test the efficiency of two different preparation methods of the bimetallic photocatalysts. In the first method, TiFeO particles were prepared by co-precipitation, as in the case of CuFeO and CoFeO, while in the second method, the particles were prepared by impregnation. The performances of these photocatalysts were compared to that of pure TiO_2 (synthesised by the sol-gel procedure according to [30]), and commercial TiO_2 (P25) (Figure 5b).

Independently of the preparation method, the prepared MNP containing Ti coated with carbon had a better efficiency than TiO_2 synthesised by the sol-gel procedure and more unsatisfactory performance than P25. The photocatalyst prepared by the second method revealed a slightly higher OMA removal rate than the one obtained by the first method. Again, the observation correlates with a higher amount of carbon.

It is worth noting that all the modified samples underperformed sample C@FeO_CVD850, suggesting that it is not worth introducing a new metal in FeO before coating by CVD. Similarly to samples treated by CVD at 750 °C, we encapsulated MNP with carbon nanotubes and nanofibers after the CVD process at 850 °C, suggesting that the carbon phase is mainly responsible for the efficiency rather than MNP composition.

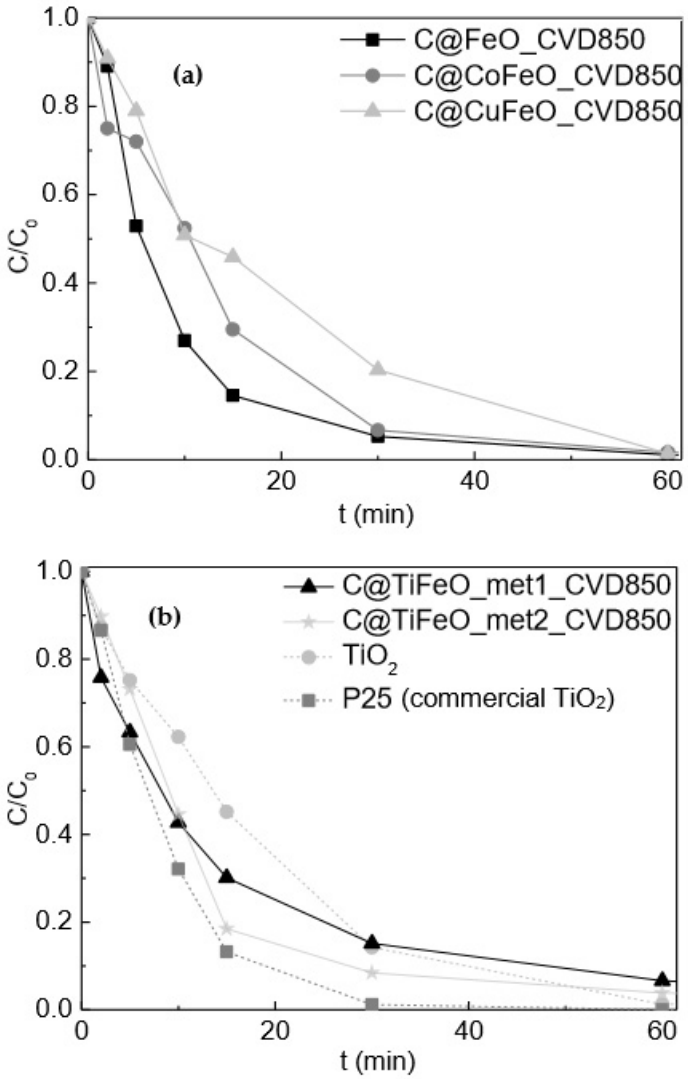

Figure 5. (**a**) OMA removal by PCO in the presence of MNP coated by CVD at 850 °C and (**b**) in the presence of Ti-based materials.

2.5. Testing the Removal Efficiency under Different Conditions

To better understand the processes evolving during OMA removal by PCO, additional experiments in the presence of the best catalyst, C@FeO_CVD850, were carried out. PCO resulting from the combination of two AOPs (ozonation and photocatalysis), potentiating the occurrence of synergetic effects. Thus, we compared the resulting levels of OMA removal in adsorption, catalytic ozonation and photocatalysis experiments performed under the same experimental conditions (Figure 6).

Adsorption on C@FeO_CVD850 was negligible. C@FeO_CVD850 was not a suitable catalyst for ozonation, removing only 10% of OMA after 60 min of reaction. The low catalytic activity verified during ozonation can be related to the small surface area of the C@FeO_CVD850 sample. On the other hand, the tested catalyst was photoactive, achieving a pollutant degradation of approximately 70% after 60 min of reaction. The verified catalytic activity probably resulted from the available electrons on the catalyst surface caused by the presence of metal oxide. However, the verified efficiency during PCO is higher than the sum of the performances obtained during photocatalysis and catalytic ozonation, suggesting the presence of a synergy when O_3, light and C@FeO_CVD850 were acting simultaneously. The high catalytic activity verified with the best sample resulted mainly due to the presence of the carbon phase. However, the presence of a metal oxide on the catalyst surface slightly contributed to

the removal achieved by PCO. A more significant number of radicals is expected to generate when O_3, UV radiation and an appropriate catalyst are together, accounting for the high activity observed [30,31].

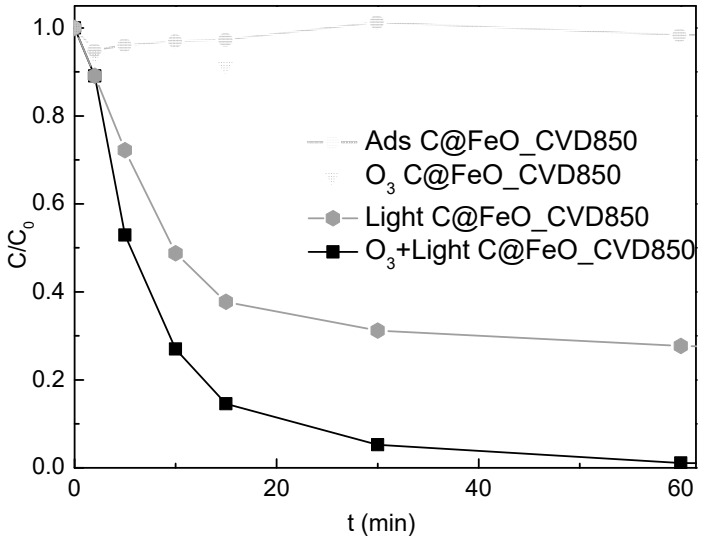

Figure 6. OMA removal by adsorption (Ads), catalytic ozonation, photocatalysis and PCO in the presence of C@FeO_CVD850.

The reutilisation of C@FeO_CVD850 was carried out to study the eventual deactivation during photocatalytic ozonation. For these experiments, a new solution was admitted to the reactor at the beginning of every reaction cycle (Figure 7).

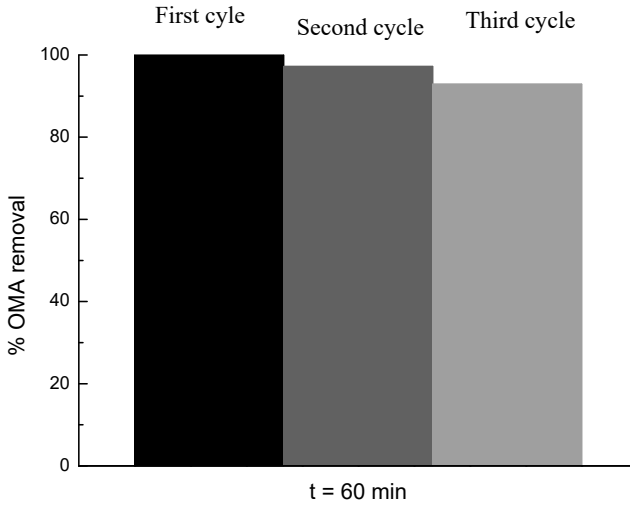

Figure 7. Runs of photocatalytic ozonation in the presence of C@FeO_CVD850.

Although there is a systematic decrease in the conversion of OMA after 60 min of reaction with C@FeO_CVD850, the photocatalyst remained active even after three cycles. A 7% loss in performance was observed from the first use to the third cycle of experiments (respectively 100%, 97% and 93% conversion measured in the consecutive runs). Since adsorption of OMA was demonstrated to be negligible, this is probably due to overoxidation of the surface by the accumulation of reactive oxygen species that will hinder the semiconductive optical properties of the material as well the active sites for ozone adsorption.

2.6. Removal of Other Pollutants by PCO

To assess the efficiency of PCO in the presence of C@FeO_CVD850 for the degradation of more complex compounds, we selected three representatives of different classes of pollutants namely: C.I. Reactive Blue 5 (DYE) as model of a textile effluent, aniline (ANL) as an example of an industrial pollutant and metolachlor (MTLC) as an emergent compound provided from the most widely used class of herbicides. Since direct ozonation is efficient to degrade compounds containing either an activated aromatic ring or double bonds, O_3 can remove these pollutants, but it presents limitations to achieve high mineralisation degrees [32,33]. The conversion of the selected contaminants over 30 min of PCO in the presence of C@FeO_CVD850 is represented in Figure 8a–c. As expected, the presence of O_3 was enough to remove the selected parent pollutants in a short reaction time. In the case of the DYE removal, the three processes had similar efficiencies. However, for ANL and MTLC, PCO was revealed to be more effective than single ozonation.

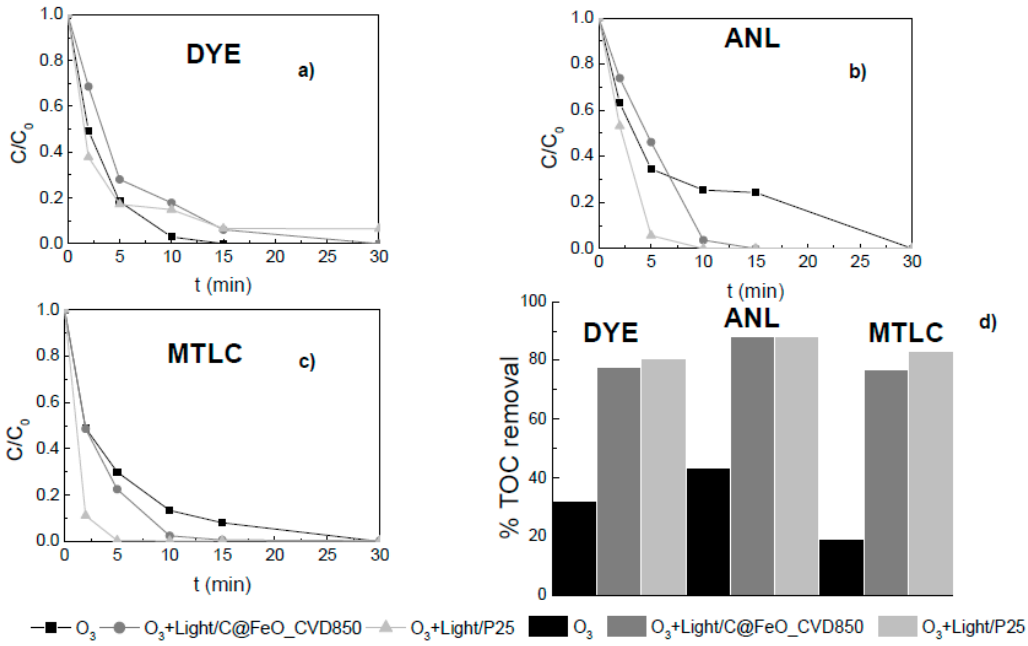

Figure 8. Evolution of dimensionless concentration of C.I. Reactive Blue 5 (DYE) (**a**), aniline (ANL) (**b**) and metolachlor (MTLC) (**c**) over 30 min, and the respective total organic carbon (TOC) removal after 180 min of reaction (**d**) by single ozonation and photocatalytic ozonation in the presence of C@FeO_CVD850 and P25.

We compared the degree of mineralisation measured in terms of total organic carbon (TOC) removal after 180 min for three standard processes: single ozonation, PCO in the presence of P25, and PCO in the presence of C@FeO_CVD850 (Figure 8d). In terms of mineralization level, the combination of O_3 with radiation and a catalyst was necessary to improve the organic matter removal. The prepared MNP coated with carbon by CVD at 850 °C showed a TOC removal between 78% and 88% after 180 min of reaction, suggesting a high rate of degradation and conversion into CO_2 and H_2O.

The photocatalyst C@FeO_CVD850 showed no lesser performance than the commercial benchmark P25 (TiO_2) in the PCO but had the additional advantage of possessing magnetic properties to facilitate separation from the aqueous solution.

3. Materials and Methods

3.1. Catalyst Preparation and Characterisation

The co-precipitation method was used to prepare FeO, CoFeO and CuFeO. Further details about FeO and CoFeO preparation can be found elsewhere [13]. For the synthesis of CuFeO, the method followed the CoFeO procedure, but replaced the cobalt precursor with $Cu(NO_3)_2{\cdot}3H_2O$.

AgFeO was prepared by incipient wetness by dropping $AgNO_3$ into the FeO support. The silver content was 5% wt. After that, the sample was dried at 100 °C for 24 h and then thermal treated under nitrogen flow at 200 °C for 2 h.

As Ti-based materials are highly active for PCO, two FeTiO samples were prepared. Sample FeTiO_m1 was obtained as CoFeO and CuFeO samples using $Ti[OCH(CH_3)_2]_4$ as a Ti precursor instead of Co and Cu precursors. Sample FeTiO_m2 was synthesised by dispersing FeO in alcohol for 1 h under ultrasonication [34], followed by the addition of a mixture containing ammonia (55%) and deionised water (45%), and ultrasonication for 1 h. The resulting particles were added into the alcohol solution of $Ti[OCH(CH_3)_2]_4$, and the mixture was stirred for 30 min. After that, 0.4 mL HNO_3 was added and the mixture was vigorously stirred for 4 h and then ultrasonicated for 1 h. The solid was obtained by magnetic separation and thermal treated under nitrogen flow at 450 °C for 1 h.

After the synthesis, the obtained MNP were coated with carbon by CVD using the approach reported elsewhere [13]. Briefly, the MNP were thermal treated under nitrogen flow up to 400 °C and then the reduction step was carried out in a hydrogen atmosphere for 2 h. After that, the temperature was increased up to 750 °C for sample C@MNP_CVD750, or 850 °C for sample C@MNP_CVD850 (where MNP can be FeO, CoFeO, CuFeO or TiFeO) to coat the magnetic nanoparticles with carbon using ethane as a carbon precursor.

The samples were characterised by different techniques. The BET surface areas of the prepared samples were calculated from N_2 equilibrium adsorption/desorption isotherms, determined to be −196 °C with a Quantachrome Instruments NOVA 4200e apparatus. TG analysis was carried out to determine the relative amount of metals in the samples, and for that purpose, an STA 409 PC/4/H Luxx Netzsch thermal analyser was used. TEM micrographs were obtained using an LEO 906E microscope operating with an accelerating voltage of 120 kV. The phase purity of the samples was inferred by XRD analyses, over a range of 2θ = 20°–80° with a Philips X'Pert MPD diffractometer (Cu-Ka = 0.15406 nm). The Rietveld refinement was used to evaluate the results.

3.2. Photocatalytic Ozonation Reactions

Experiments of PCO were carried out in a glass immersion photochemical reactor loaded with 0.5 g L^{-1} of catalyst concentration, as described elsewhere [30]. The reactions were performed with the following initial concentrations: $C_{0,\ OMA}$ = 89.05 mg L^{-1}, $C_{0,\ ANL}$ = 93.13 mg L^{-1}, $C_{0,\ MTLC}$ = 283.80 g L^{-1} and $C_{0,\ DYE}$ = 100 mg L^{-1}. The radiation source was a Heraeus TQ 150 medium-pressure mercury vapour lamp placed axially with a DURAN 50® glass cooling jacket positioned around the lamp, resulting in the main emission lines at λ_{exc} = 365 nm, 405 nm, 436 nm, 546 nm and 578 nm, which correspond to a spectral energy range between 2.15 eV and 3.40 eV. The gas was bubbled into the reactor at a constant flow rate (150 cm^3 min^{-1}) and inlet O_3 concentration (50 g m^{-3}). O_3 was produced from pure O_2 in a BMT 802X ozone generator. The concentration of O_3 in the gas phase was monitored with a BMT 964 O_3 analyser. Due to the magnetic behaviour of the prepared samples, the catalysts were easily recovered from the solution through the application of a magnetic field after each reaction.

The performance of the different catalysts during OMA removal by PCO was evaluated in terms of pollutant concentration as determined by high performance liquid chromatography (HPLC) analysis with an Hitachi Elite Lachrom system equipped with an ultraviolet detector. The stationary phase was an Altech AO-100 column working at room temperature under isocratic elution with H_2SO_4 (5 mM) at a flow rate of 0.5 cm^3 min^{-1}. The injection volume was 15 µL, and the detector

wavelength was 200 nm [30]. The concentration of DYE was determined bya PG Instruments T60 UV-Vis spectrophotometer at the maximum absorption wavelength (630 nm). ANL and MTLC concentrations were determined using an HPLC Hitachi Elite Lachrom system equipped with a diode array detector (DAD). For ANL concentration, the stationary phase was a Lichrocart Purospher Star column working at room temperature under isocratic elution with 40% water and 60% methanol at a flow rate of 1 mL min^{-1}, an injection volume of 40 µL and the wavelength used was 200 nm. In the case of MTLC, the separation of the pollutant was attained by using the same column as used for ANL but with an isocratic mobile phase containing 60% acetonitrile and 40% water.

In the case of DYE, ANL and MTLC, the catalytic activity was also evaluated in terms of mineralization degree by the determination of TOC removal by a Shimadzu TOC-L total organic carbon analyser coupled with an ASI-L autosampler using the non-purgeable organic carbon (NPOC) method.

4. Conclusions

The use of magnetic nanoparticles (MNP) of FeO and their Ag and Cu bimetallic derivatives was successfully demonstrated for the photocatalytic ozonation (PCO) of oxamic acid (OMA), a model compound, for the first time. MNP also presented high catalytic activity during degradation of other representative pollutants.

The CVD coating procedure proves to be a simple and accessible technique to efficiently carbon-coat FeO MNP, as well as their bimetallic derivatives. This procedure allowed us to take advantage of the catalytic properties of the carbon materials, in addition to the efficient recovery attained due to their magnetic character.

The increase in performance associated with the temperature of CVD demonstrated the importance of the carbon coating in the photocatalytic process. Notably, it showed that more critical than the magnetic core was the quality (amount) of the carbon coating. The best results correlate with the increasing carbon content of the surface associated with higher CVD temperatures.

The modification of the FeO core with other metals did not represent an advantage for the carbon-coated MNP. The pristine C@FeO_CVD850 displayed an obvious synergy in PCO owing to the thermal and coating effects. C@FeO_CVD850 was quickly removed from the media and successfully applied in consecutive runs, presenting a rapid recycling operation mode due to its magnetic character. The successive PCO experimental runs with OMA showed that the C@FeO_CVD850 photocatalyst is very stable, remaining highly active after three initial cyclic tests.

The PCO of other pollutants (model compound of a textile effluent, an industrial pollutant and an emergent contaminant) revealed that the synergic effect evidenced by C@FeO_CVD850 enhanced the organic matter removal of the aqueous solutions compared to single ozonation, with almost complete mineralization being achieved.

Compared to the photocatalytic performance of commercial P25 (TiO2), no significant differences were observed, suggesting that C@FeO_CVD850 emerged as a remarkable alternative to remove a wide range of pollutants by PCO, due to its additional capacity of being efficiently recovered from the solution (by means of its magnetic properties), which is very appealing in terms of practical applications. Therefore, this work successfully answered to the constant challenge of developing a catalyst with similar performance to P25.

In conclusion, C@FeO_CVD850 emerges as a promising catalyst in the PCO process of an extensive class of pollutants with the advantage of being easily recovered from the media.

Author Contributions: Conceptualization, C.A.O. and O.S.G.P.S.; Investigation, C.A.O. and P.S.F.R.; Resources, M.F.R.P. and J.L.F.; Writing—Original Draft Preparation, C.A.O.; Validation and Writing—Review and Editing, O.S.G.P.S., M.F.R.P. and J.L.F.

Funding: This work is a result of: Project "AIProcMat@N2020-Advanced Industrial Processes and Materials for a Sustainable Northern Region of Portugal 2020", with the reference NORTE-01-0145-FEDER-000006, supported by Norte Portugal Regional Operational Programme (NORTE 2020), under the Portugal 2020 Partnership Agreement, through the European Regional Development Fund (ERDF); Associate Laboratory LSRE-LCM-UID/EQU/50020/2019-funded by national funds through FCT/MCTES (PIDDAC).

Conflicts of Interest: The authors declare no conflict of interest.

References

1. Mehrjouei, M.; Müller, S.; Möller, D. A review on photocatalytic ozonation used for the treatment of water and wastewater. *Chem. Eng. J.* **2015**, *263*, 209–219. [CrossRef]
2. Chávez, A.M.; Ribeiro, A.R.; Moreira, N.F.F.; Silva, A.M.T.; Rey, A.; Álvarez, P.M.; Beltrán, F.J. Removal of Organic Micropollutants from a Municipal Wastewater Secondary Effluent by UVA-LED Photocatalytic Ozonation. *Catalysts* **2019**, *9*, 472. [CrossRef]
3. Mills, A.; Lee, S.K. A web-based overview of semiconductor photochemistry-based current commercial applications. *J. Photochem. Photobiol. A Chem.* **2002**, *152*, 233–247. [CrossRef]
4. Chen, X.; Gambhir, S.S.; Cheon, J. Theranostic Nanomedicine. *Acc. Chem. Res.* **2011**, *44*, 841. [CrossRef] [PubMed]
5. Xie, J.; Liu, G.; Eden, H.S.; Ai, H.; Chen, X. Surface-Engineered Magnetic Nanoparticle Platforms for Cancer Imaging and Therapy. *Acc. Chem. Res.* **2011**, *44*, 883–892. [CrossRef]
6. Suber, L.; Marchegiani, G.; Olivetti, E.; Celegato, F.; Coisson, M.; Tiberto, P.M.; Allia, P.; Barrera, G.; Pilloni, L.; Barba, L.; et al. Pure magnetic hard fct FePt nanoparticles: Chemical synthesis, structural and magnetic properties correlations. *Mater. Chem. Phys.* **2014**, *144*, 186–193. [CrossRef]
7. Long, Y.; Xie, M.; Niu, J.; Wang, P.; Ma, J. Preparation of acid–base bifunctional core–shell structured Fe3O4@SiO2 nanoparticles and their cooperative catalytic activity. *Appl. Surf. Sci.* **2013**, *277*, 288–292. [CrossRef]
8. Xu, X.; Wu, H.; Li, Z.; Sun, X.; Wang, Z. Iron oxide-silver magnetic nanoparticles as simple heterogeneous catalysts for the direct inter/intramolecular nucleophilic substitution of π-activated alcohols with electron-deficient amines. *Tetrahedron* **2015**, *71*, 5254–5259. [CrossRef]
9. Shokouhimehr, M. Magnetically Separable and Sustainable Nanostructured Catalysts for Heterogeneous Reduction of Nitroaromatics. *Catalyst* **2015**, *5*, 534–560. [CrossRef]
10. Hu, J.; Chen, G.; Lo, I.M.C. Selective Removal of Heavy Metals from Industrial Wastewater Using Maghemite Nanoparticle: Performance and Mechanisms. *J. Environ. Eng.* **2006**, *132*, 709–715. [CrossRef]
11. Ali, Q.; Ahmed, W.; Lal, S.; Sen, T. Novel Multifunctional Carbon Nanotube Containing Silver and Iron Oxide Nanoparticles for Antimicrobial Applications in Water Treatment. *Mater. Today Proc.* **2017**, *4*, 57–64. [CrossRef]
12. Funari, V.; Mantovani, L.; Vigliotti, L.; Tribaudino, M.; Dinelli, E.; Braga, R. Superparamagnetic iron oxides nanoparticles from municipal solid waste incinerators. *Sci. Total Environ.* **2018**, *621*, 687–696. [CrossRef]
13. Pereira, L.; Dias, P.; Soares, O.; Ramalho, P.; Pereira, M.; Alves, M.; Pereira, M.F. Synthesis, characterization and application of magnetic carbon materials as electron shuttles for the biological and chemical reduction of the azo dye Acid Orange 10. *Appl. Catal. B Environ.* **2017**, *212*, 175–184. [CrossRef]
14. Mahmoodi, N.M. Photocatalytic ozonation of dyes using copper ferrite nanoparticle prepared by co-precipitation method. *Desalination* **2011**, *279*, 332–337. [CrossRef]
15. Mahmoodi, N.M.; Bashiri, M.; Moeen, S.J. Synthesis of nickel–zinc ferrite magnetic nanoparticle and dye degradation using photocatalytic ozonation. *Mater. Res. Bull.* **2012**, *47*, 4403–4408. [CrossRef]
16. Yin, J.; Liao, G.; Zhou, J.; Huang, C.; Ling, Y.; Lu, P.; Li, L. High performance of magnetic $BiFeO_3$ nanoparticle-mediated photocatalytic ozonation for wastewater decontamination. *Sep. Purif. Technol.* **2016**, *168*, 134–140. [CrossRef]
17. Figueiredo, J.L.; Pereira, M.F.R. Carbon as Catalyst. In *Carbon Materials for Catalysis*; Serp, P., Figueiredo, J.L., Eds.; John Wiley & Sons, Inc.: Hoboken, NJ, USA, 2009; pp. 177–217.
18. Cai, Y.; Qin, J.; Wei, F.; Xu, C.; Yao, Y.; Lu, F.; Wang, S. Magnetic $ZnFe_2O_4$–C_3N_4 Hybrid for Photocatalytic Degradation of Aqueous Organic Pollutants by Visible Light. *Ind. Eng. Chem. Res.* **2014**, *53*, 17294–17302.
19. Hussain, I.; Zhang, Y.; Li, M.; Huang, S.; Hayat, W.; He, L.; Du, X.; Liu, G.; Du, M. Heterogeneously degradation of aniline in aqueous solution using persulfate catalyzed by magnetic $BiFeO_3$ nanoparticles. *Catal. Today* **2018**, *310*, 130–140. [CrossRef]
20. De Oliveira, J.S.; Salla, J.D.; Kuhn, R.C.; Jahn, S.L.; Foletto, E.L. Catalytic Ozonation of Melanoidin in Aqueous Solution over $CoFe_2O_4$ Catalyst. *Mater. Res. Ibero Am. J.* **2019**, *22*, 1–9. [CrossRef]

21. Wang, J.; Shao, X.; Zhang, Q.; Ma, J.; Ge, H. Preparation and photocatalytic application of magnetic Fe2O3/SBA-15 nanomaterials. *J. Mol. Liq.* **2018**, *260*, 304–312. [CrossRef]
22. Wang, Z.; Ma, H.; Zhang, C.; Feng, J.; Pu, S.; Ren, Y.; Wang, Y. Enhanced catalytic ozonation treatment of dibutyl phthalate enabled by porous magnetic Ag-doped ferrospinel $MnFe_2O_4$ materials: Performance and mechanism. *Chem. Eng. J.* **2018**, *354*, 42–52. [CrossRef]
23. Ortiz-Quiñonez, J.L.; Pal, U.; Villanueva, M.S. Structural, Magnetic, and Catalytic Evaluation of Spinel Co, Ni, and Co–Ni Ferrite Nanoparticles Fabricated by Low-Temperature Solution Combustion Process. *ACS Omega* **2018**, *3*, 14986–15001. [CrossRef]
24. Vinosel, V.M.; Anand, S.; Janifer, M.A.; Pauline, S.; Dhanavel, S.; Praveena, P.; Stephen, A. Enhanced photocatalytic activity of Fe3O4/SnO2 magnetic nanocomposite for the degradation of organic dye. *J. Mater. Sci. Mater. Electron.* **2019**, *30*, 9663–9677. [CrossRef]
25. Shi, J.; Feng, S.; Chen, T.; Wu, F.; Guo, W.; Li, Y.; Zhao, P. Novel rattle-type magnetic Fe_3O_4@Ag@H-BiOCl photocatalyst with enhanced visible light-driven photocatalytic activity. *J. Mater. Sci. Mater. Electron.* **2018**, *29*, 10204–10213. [CrossRef]
26. Orge, C.; Faria, J.; Pereira, M.; Pereira, M.F. Removal of oxalic acid, oxamic acid and aniline by a combined photolysis and ozonation process. *Environ. Technol.* **2014**, *36*, 1075–1083. [CrossRef]
27. Sampaio, M.J.; Lima, M.J.; Baptista, D.L.; Silva, A.M.; Silva, C.G.; Faria, J.L. Ag-loaded ZnO materials for photocatalytic water treatment. *Chem. Eng. J.* **2017**, *318*, 95–102. [CrossRef]
28. Yao, Y.; Li, G.; Ciston, S.; Lueptow, R.M.; Gray, K.A. Photoreactive TiO_2/carbon nanotube composites: Synthesis and reactivity. *Environ. Sci. Technol.* **2008**, *42*, 4952–4957. [CrossRef]
29. Kumar, M.; Ando, Y. Chemical vapor deposition of carbon nanotubes: A review on growth mechanism and mass production. *J. Nanosci. Nanotechnol.* **2010**, *10*, 3739–3758. [CrossRef]
30. Orge, C.; Pereira, M.F.; Faria, J. Photocatalytic ozonation of model aqueous solutions of oxalic and oxamic acids. *Appl. Catal. B Environ.* **2015**, *174*, 113–119. [CrossRef]
31. Orge, C.A.; Soares, O.S.G.; Faria, J.L.; Pereira, M.F.R. Synthesis of TiO_2-Carbon Nanotubes through ball-milling method for mineralization of oxamic acid (OMA) by photocatalytic ozonation. *J. Environ. Chem. Eng.* **2017**, *5*, 5599–5607. [CrossRef]
32. Orge, C.; Faria, J.; Pereira, M.; Pereira, M.F.; Orge, C. Photocatalytic ozonation of aniline with TiO_2-carbon composite materials. *J. Environ. Manag.* **2017**, *195*, 208–215. [CrossRef] [PubMed]
33. Orge, C.; Pereira, M.; Faria, J.; Orge, C.; Pereira, M.F. Photocatalytic-assisted ozone degradation of metolachlor aqueous solution. *Chem. Eng. J.* **2017**, *318*, 247–253. [CrossRef]
34. Tang, Y.; Zhang, G.; Liu, C.; Luo, S.; Xu, X.; Chen, L.; Wang, B. Magnetic TiO_2-graphene composite as a high-performance and recyclable platform for efficient photocatalytic removal of herbicides from water. *J. Hazard. Mater.* **2013**, *252*, 115–122. [CrossRef] [PubMed]